Supporting Information

Integrated Three-Dimensional Carbon Paper/Carbon Tubes/Cobalt-Sulfide Sheets as an Efficient Electrode for Overall Water Splitting

Jun Wang,[†,‡] Hai-xia Zhong,[†,‡] Zhong-li Wang,[†] Fan-lu Meng,[†] Xin-bo Zhang[*,†]

[†]State Key Laboratory of Rare Earth Resource Utilization, Changchun Institute of Applied Chemistry, Chinese Academy of Sciences, Changchun 130022, P. R. China

[‡]University of Chinese Academy of Sciences, Beijing 100049, P. R. China

Chemicals. Zinc nitrate hexahydrate ($Zn(NO_3)_2 \cdot 6H_2O$, 99%), potassium permanganate ($KMnO_4$, 99%), cobalt nitrate hexahydrate ($Co(NO_3)_2 \cdot 6H_2O$, 99%), hexamethylenetetramine ($C_6H_{12}N_4$, ≥99.0%), tris(hydroxymethyl)aminomethane ($C_4H_{11}NO_3$, Tris, ≥99.0%), thiourea (CH_4N_2S, 99%), ammonia solution ($NH_3 \cdot H_2O$, 25-28%), hydrochloric acid (HCl, 36%-38%), anhydrous ethanol (C_2H_5OH) were purchased from Beijing Chemical Works. Potassium hydroxide (KOH, 98%) was purchased from Aladdin Reagent. Dopamine hydrochloride, Pt/C (20 wt%) and RuO_2 were purchased from Sigma-Aldrich. Nafion solution (5 wt%) was purchased from DuPont. All chemical reagents were used as received without further purification. Deionized water with the specific resistance of 18.2 MΩ·cm was obtained by reversed osmosis followed by ion-exchange and filtration.

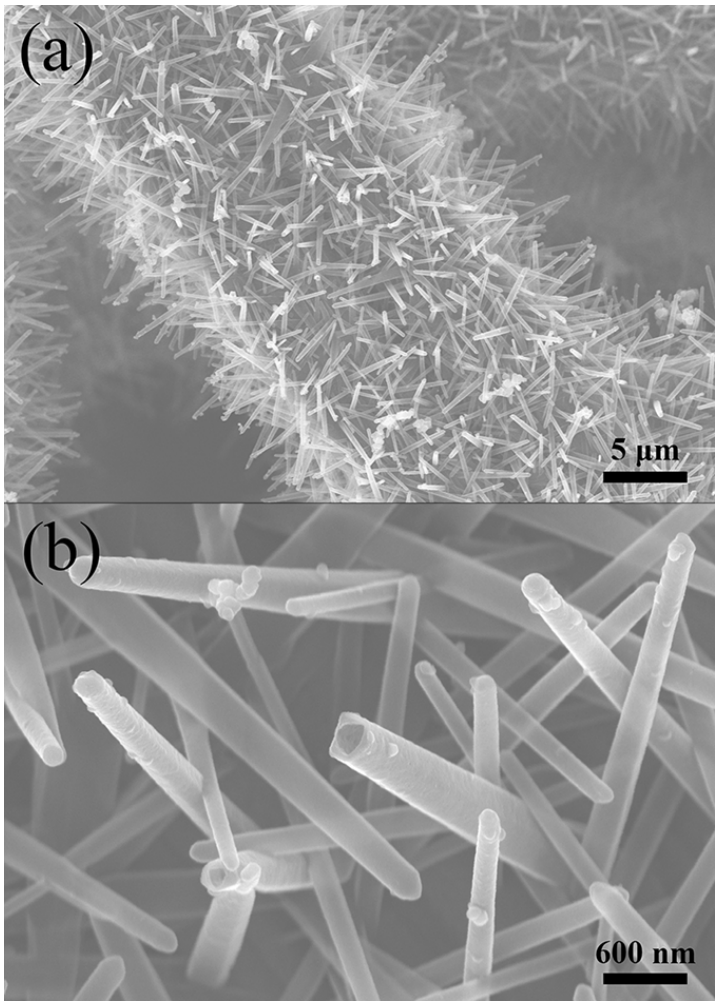

Figure S1. SEM images of CP/CTs.

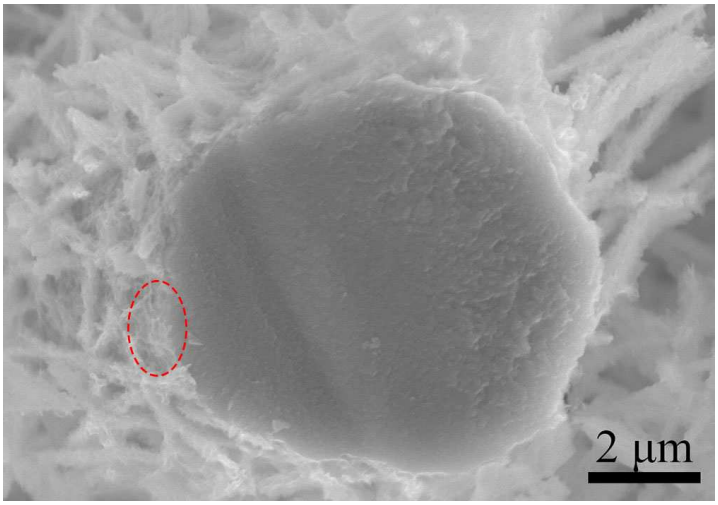

Figure S2. SEM image of the cross-sectional view of CP/CTs/Co-S sheets. The red circle indicates that Co-S sheets are also partly deposited on the skeleton of CP.

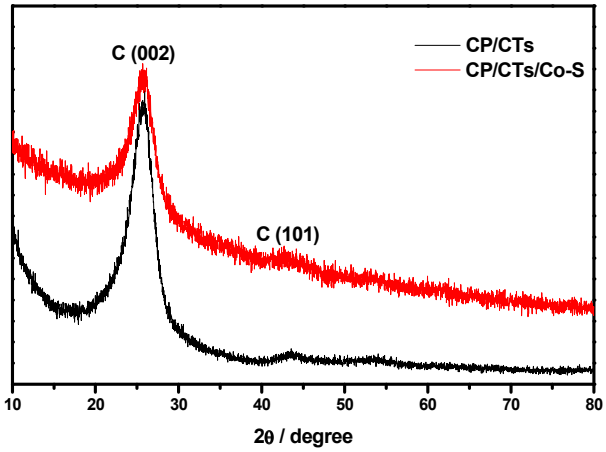

Figure S3. XRD patterns of CP/CTs and CP/CTs/Co-S.

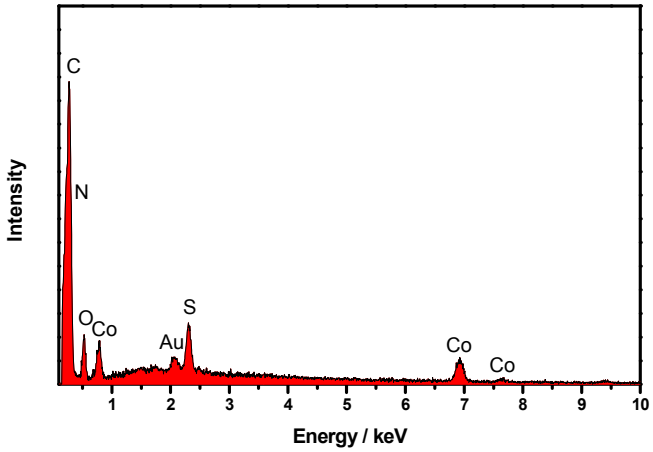

Figure S4. EDX spectrum of CP/CTs/Co-S. The Au signal is originated from the sputtered Au before test.

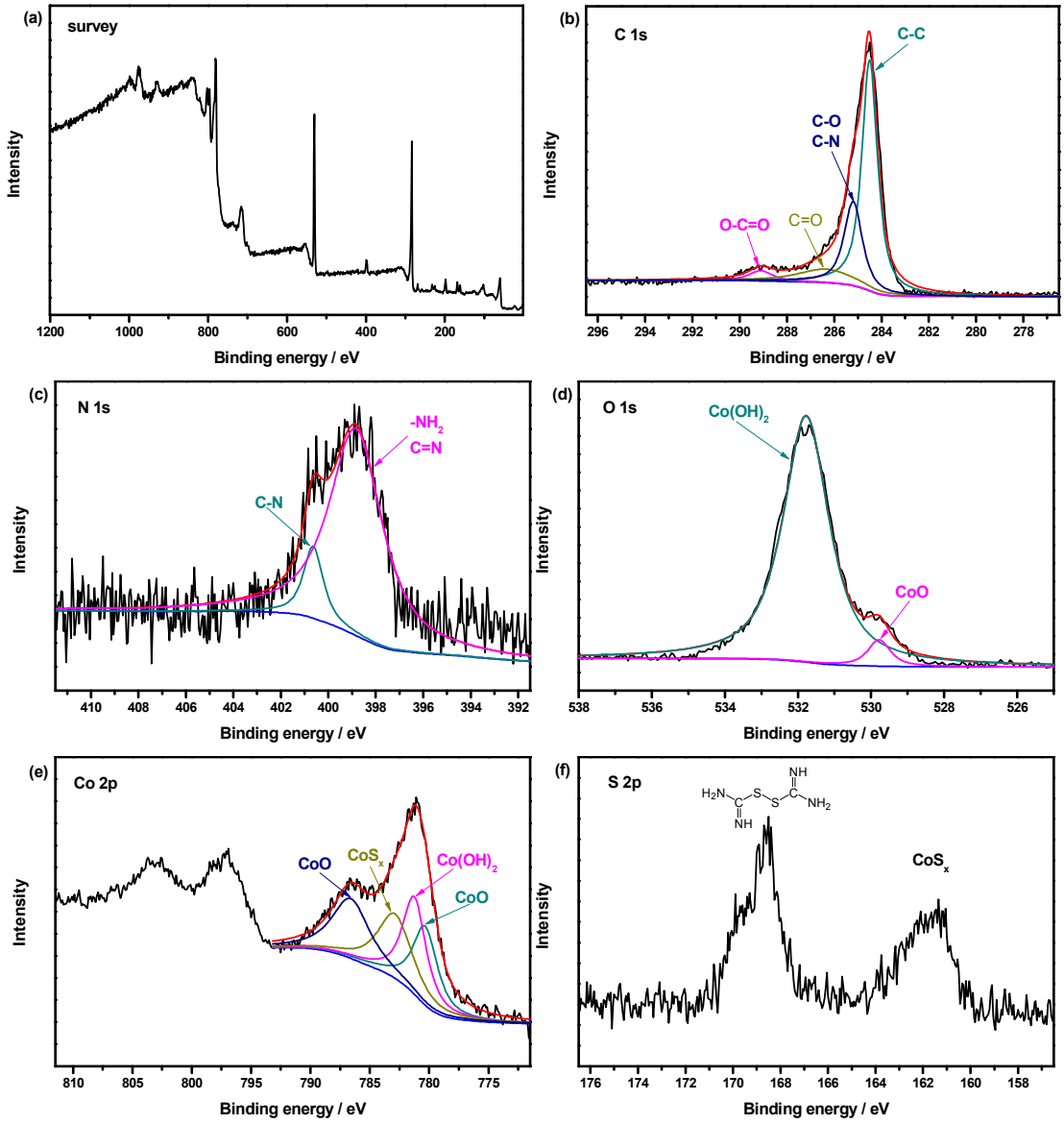

Figure S5. XPS spectra of (a) survey, (b) C 1s, (c) N 1s, (d) O 1s, (e) Co 2p, and (f) S 2p for CP/CTs/Co-S.

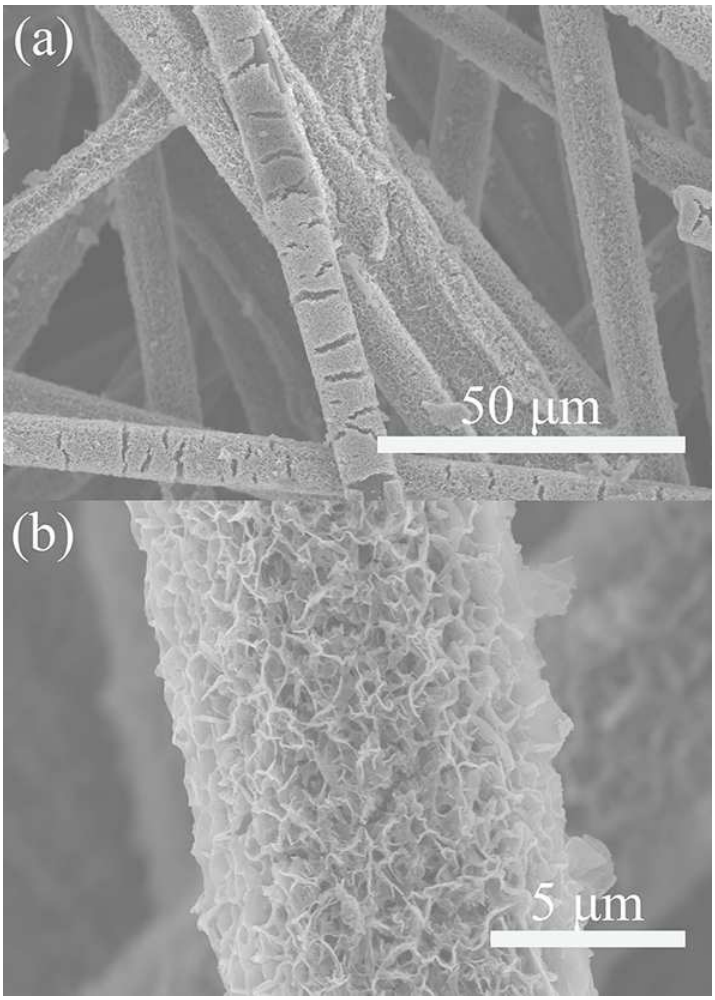

Figure S6. SEM images of CP/Co-S.

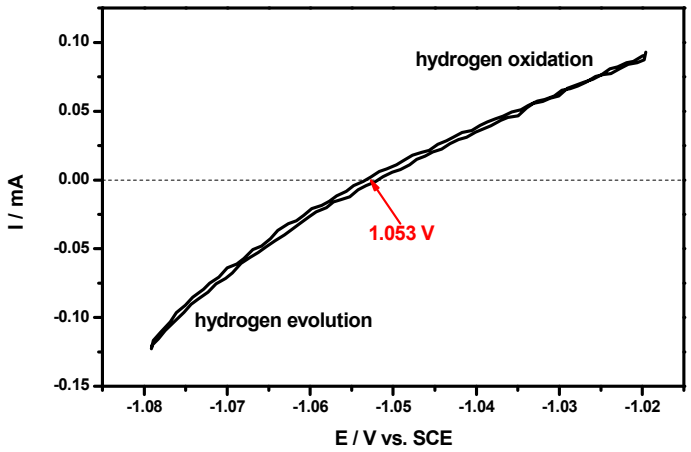

Figure S7. The calibration of SCE (saturated KCl) reference electrode with respect to RHE.

The calibration was performed in the high purity hydrogen saturated electrolyte (1 M KOH) with a Pt mesh as the working electrode. Cyclic voltammograms were run at a scan rate of 1 mV s^{-1}, and the average of the two potentials at which the current crossed zero was taken to be the thermodynamic potential for the hydrogen electrode reactions. Thus, in 1 M KOH, E (RHE) = E (SCE) + 1.053 V.

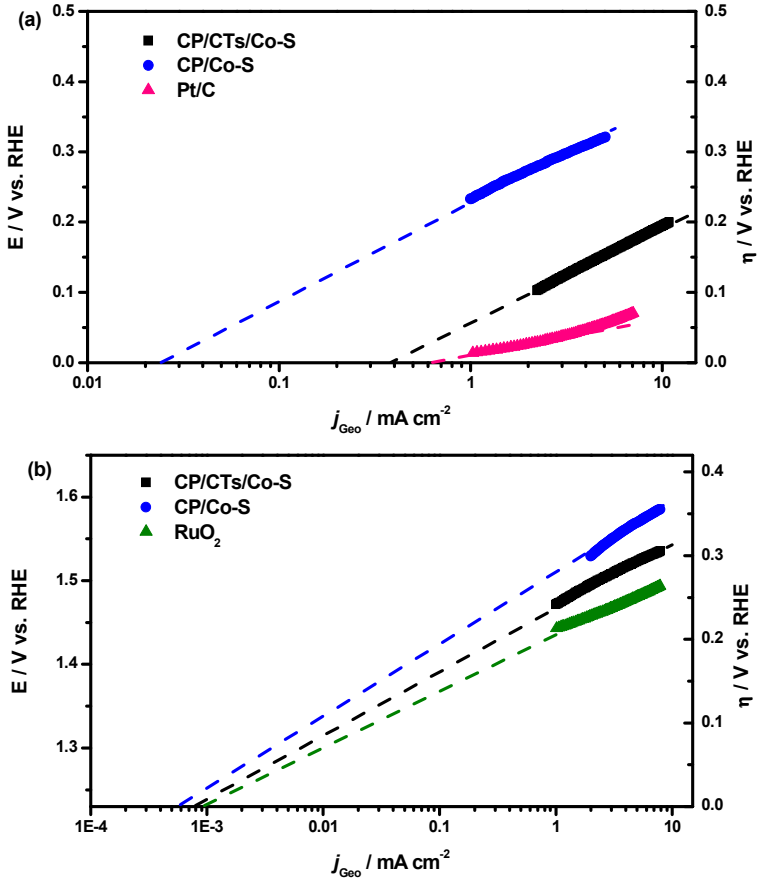

Figure S8. Exchange current densities for HER (a) and OER (b) calculated from Tafel plots by extrapolation method.

Table S1. Summary of the electrochemical activities of the catalytic electrodes for HER and OER.

	E @ j = 10 mA cm^{-2} (V)		**Tafel slope (mV dec^{-1})**		**Exchange current density (mA cm^{-2})**	
	HER	OER	HER	OER	HER	OER
CP/CTs/Co-S	-0.190	1.536	131	72	3.9×10^{-1}	8.3×10^{-4}
CP/Co-S	-0.357	1.593	138	101	2.4×10^{-2}	5.8×10^{-4}
Pt/C	-0.090		49		6.4×10^{-1}	
RuO_2		1.501		55		9.4×10^{-4}

Table S2. Summary of the electrochemical activities of the catalytic electrodes for HER.

Catalyst	Electrolyte	Loading (mg cm^{-2})	η(HER) at j = 10 mA cm^{-2} (mV)	TOF (s^{-1})	Tafel plot (mV dec^{-1})	Exchange current (mA cm^{-2})	Reference
CP/CTs/Co-S	1 M KOH	0.32	190	1.2×10^{-1} (η = 0.25 V)	131	3.9×10^{-1}	This work
FTO/Co-S	1 M KOH	0.08	> 600	$< 6.0\times10^{-3}$ (η = 0.25 V)			Ref. 1
MoP	1 M KOH	0.86	~140		48	4.6×10^{-2}	Ref. 2
MoB	1 M KOH	2.3	~220		59	2.0×10^{-3}	Ref. 3
Mo_2C	1 M KOH	~0.8	~190		54	3.8×10^{-3}	Ref. 3
MoC_x	1 M KOH	0.8	151		59	2.9×10^{-2}	Ref. 4
Ti foil/$Ni_{0.33}Co_{0.67}S_2$ NWs	1 M KOH	0.3	88		118	1.791	Ref. 5
CC/CoP	1 M KOH	0.92	209		129		Ref. 6
$Ni_{2/3}Fe_{1/3}$-rGO	1 M KOH	0.25	~560		210		Ref. 7
NiO/Ni-CNT	1 M KOH	0.28	80		82		Ref. 8
CoO_x@CN	1 M KOH	0.12	232				Ref. 9
Co-NRCNTs	1 M KOH	0.28	370				Ref. 10
Ni foam/NiFe LDH	1 M NaOH		210				Ref. 11
Ni@NC	0.1 M KOH	0.4	190				Ref. 12
MnNi	0.1 M KOH	0.28	360				Ref. 13

Table S3. Summary of the electrochemical activities of the catalytic electrodes for OER.

Catalyst	Electrolyte	Loading (mg cm^{-2})	η(OER) at j = 10 mA cm^{-2} (mV)	TOF (s^{-1})	Tafel plot (mV dec^{-1})	Exchange current (mA cm^{-2})	Reference
CP/CTs/Co-S	1 M KOH	0.32	306	1.6×10^{-2} (η = 0.3 V)	72	8.3×10^{-4}	This work
Exfoliated NiFe LDH	1 M KOH	0.07	302	5.0×10^{-2} (η = 0.3 V)	40		Ref. 14
Exfoliated CoMn LDH	1 M KOH	0.142	324	9.0×10^{-3} (η = 0.3 V)	43		Ref. 15
FTO/CoHCF	50 mM KPi/1M KNO_3			2.0×10^{-3} (η = 0.3 V)	88		Ref. 16
Zn-Co-LDH	0.1 M KOH	0.28	~520	6.1×10^{-2} (η = 0.41 V)			Ref. 17
α-$Ni(OH)_2$ Spheres	0.1 M KOH	0.2	331	3.61×10^{-2} (η = 0.35 V)	42		Ref. 18
Ti foil/$Ni_xCo_{3-x}O_4$ NWs	1 M NaOH	2.3	~370		64	8.8×10^{-6}	Ref. 19
Stainless steel/Co_3O_4	1 M KOH		~400		49	2.0×10^{-7}	Ref. 20
CoO_x@CN	1 M KOH	1	232				Ref. 9
Ti foil/$NiCo_2O_4$ NWs	1 M KOH	0.3	~370		60		Ref. 5
Ni foam/NiFe LDH	1 M NaOH		240				Ref. 11
Ni@NC	0.1 M KOH	0.4	390		40		Ref. 12
MnNi	0.1 M KOH	0.28	420				Ref. 13
Ni foam/Co_3O_4/N-rmGO	1 M KOH	1	310		67		Ref. 21
$Mn_3O_4/CoSe_2$	0.1 M KOH	0.2	450		49		Ref. 22
Cu foil/Co_3O_4C-NA	0.1 M KOH	~0.2	290		70		Ref. 23
Ti foil/$Zn_xCo_{3-x}O_4$ NWs	1 M KOH	~1	320		51		Ref. 24

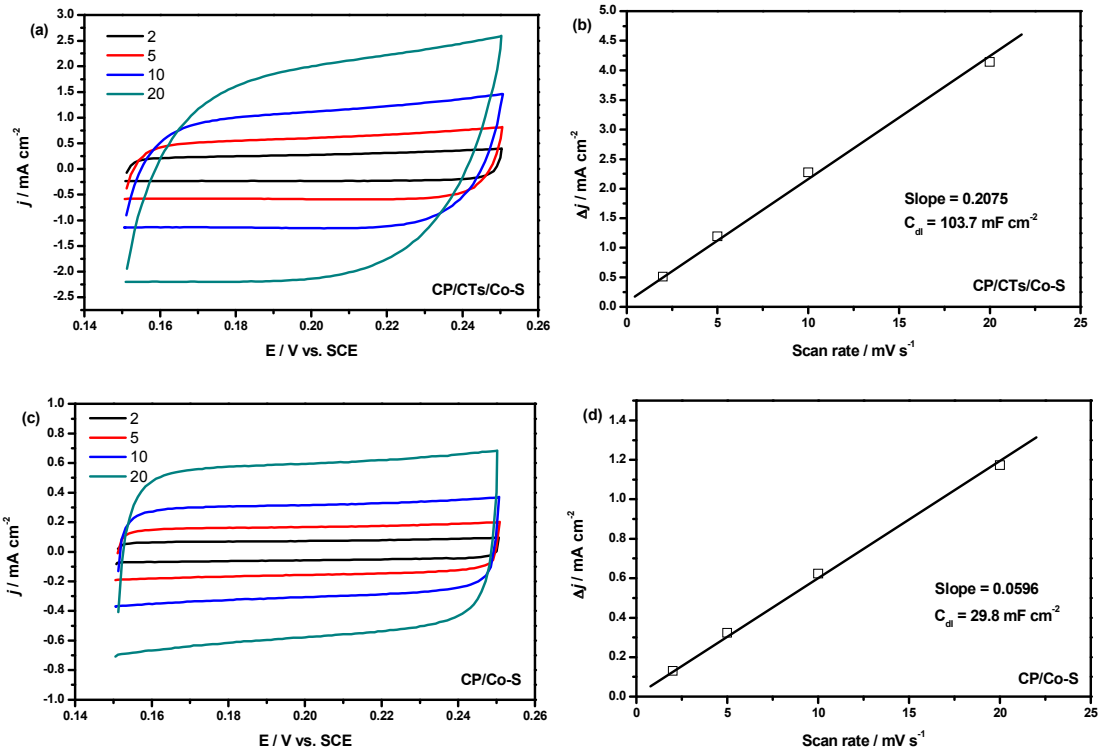

Figure S9. (a, c) Cyclic voltammograms and (b, d) the capacitive currents at 0.20 V vs. SCE as a function of scan rate for CP/CTs/Co-S and CP/Co-S in 1 M KOH.

The effective surface areas of CP/CTs/Co-S and CP/Co-S were compared by estimating their electrochemical double layer capacitances (C_{dl}) with cyclic voltammograms (CVs). CVs were performed at a potential range of 0.15-0.25 V vs. SCE where no obvious electrochemical features corresponding to the Faradic current were observed (Figure S9a and c). The capacitive currents, $\Delta j(j_a-j_c)$@0.2 V, were plotted against the scan rate (Figure S9b and d). The linear relationships were observed with the slopes twice of the C_{dl} value. Accordingly, the C_{dl} values for CP/CTs/Co-S and CP/Co-S were calculated to be 103.7 and 29.8 mF cm^{-2}, respectively.

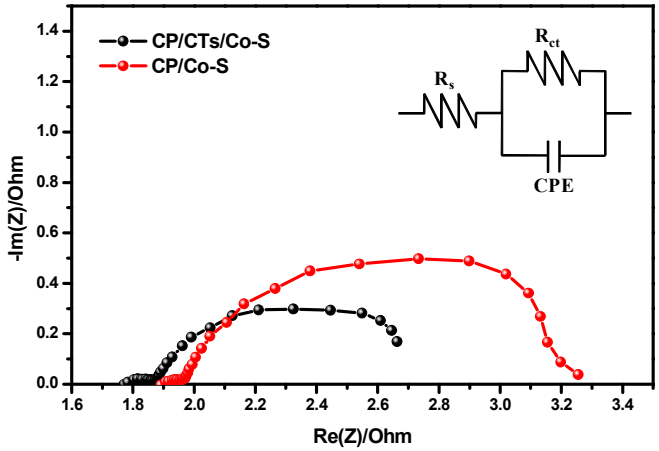

Figure S10. Electrochemical impedance spectroscopy obtained by applying an AC voltage with the amplitude of the sinusoidal voltage of 10 mV over a frequency range from 200 kHz to 100 mHz for CP/CTs/Co-S and CP/Co-S at HER overpotential of 0.2 V (Inset: the equivalent circuit diagram).

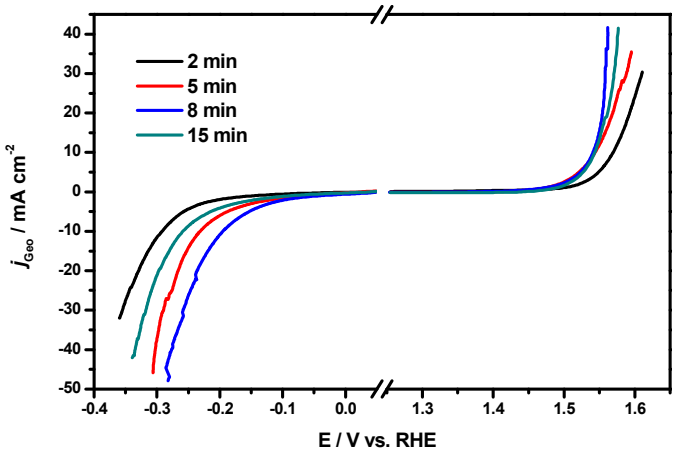

Figure S11. Polarization curves of CP/CTs/Co-S prepared with different deposition time for HER and OER in 1 M KOH with a scan rate of 2 mV s^{-1}.

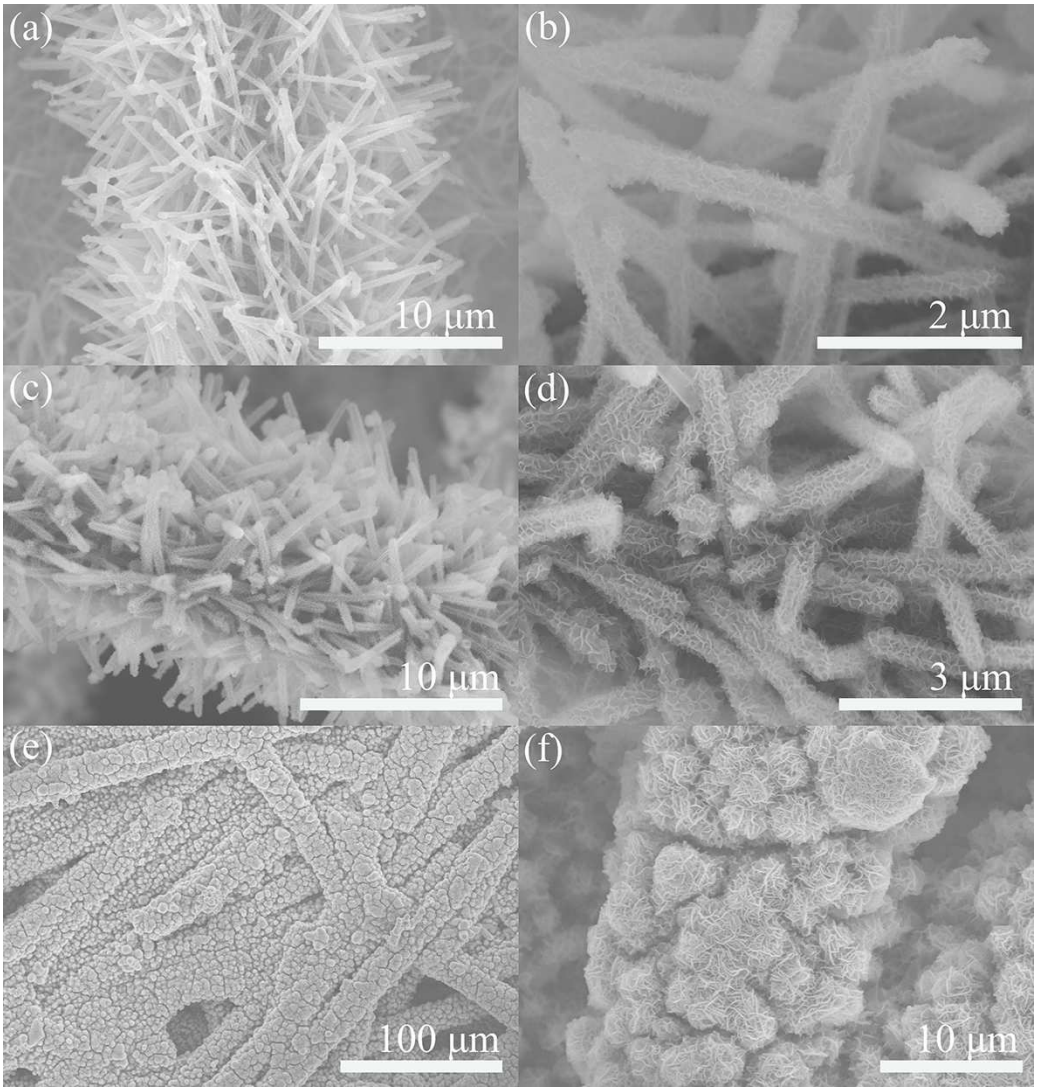

Figure S12. SEM images of CP/CTs/Co-S prepared via chronoamperometric electrodeposition at -0.9 V vs Ag/AgCl with different time: (a, b) 2, (c, d) 5, and (e, f) 15 min.

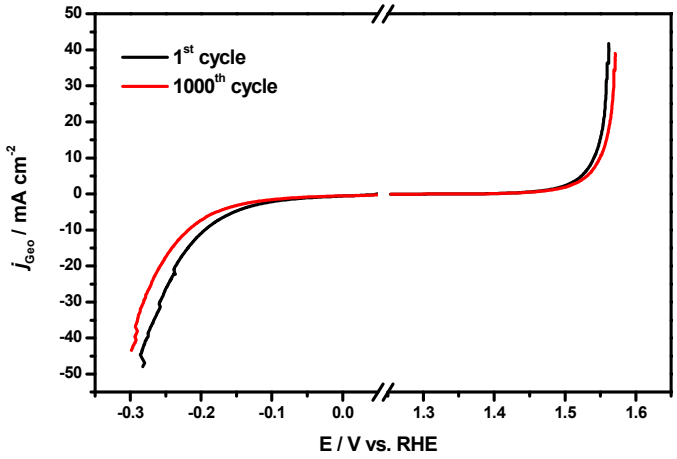

Figure S13. Polarization curves of CP/CTs/Co-S for HER and OER before and after 1000 cycles (50 mV s^{-1}) in 1 M KOH with a scan rate of 2 mV s^{-1}.

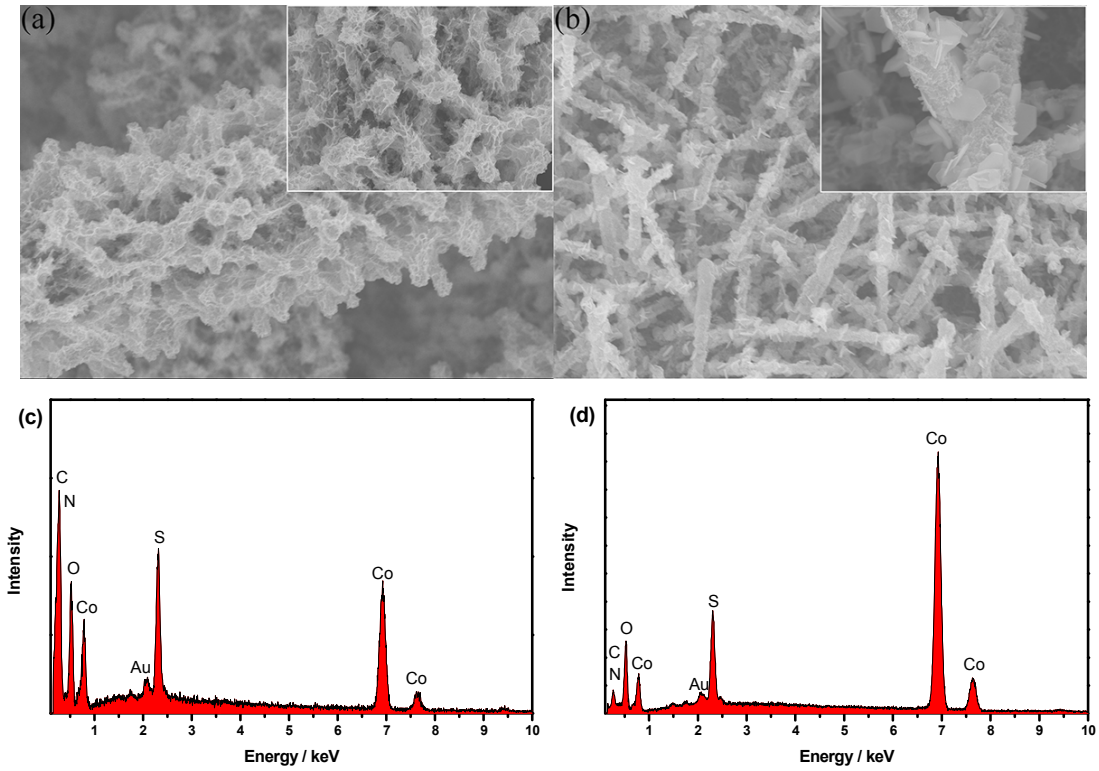

Figure S14. SEM images (a, b) and EDX spectra (c, d) of CP/CTs/Co-S after stability test for HER (a, c) and OER (b, d).

The SEM image in Figure S14a reveals that CP/CTs/Co-S almost maintains the sheet morphology after stability test for HER. And the EDX analysis (Figure S14c) shows a Co/S ratio of ~1.6, suggesting a small amount of S loss. However, after OER process, the formation of many regular plates on the surface of CTs is observed (Figure S14b) and the Co/S ratio is increased to ~5 (Figure S14d), indicating the weak stability of CoS_x under OER condition.

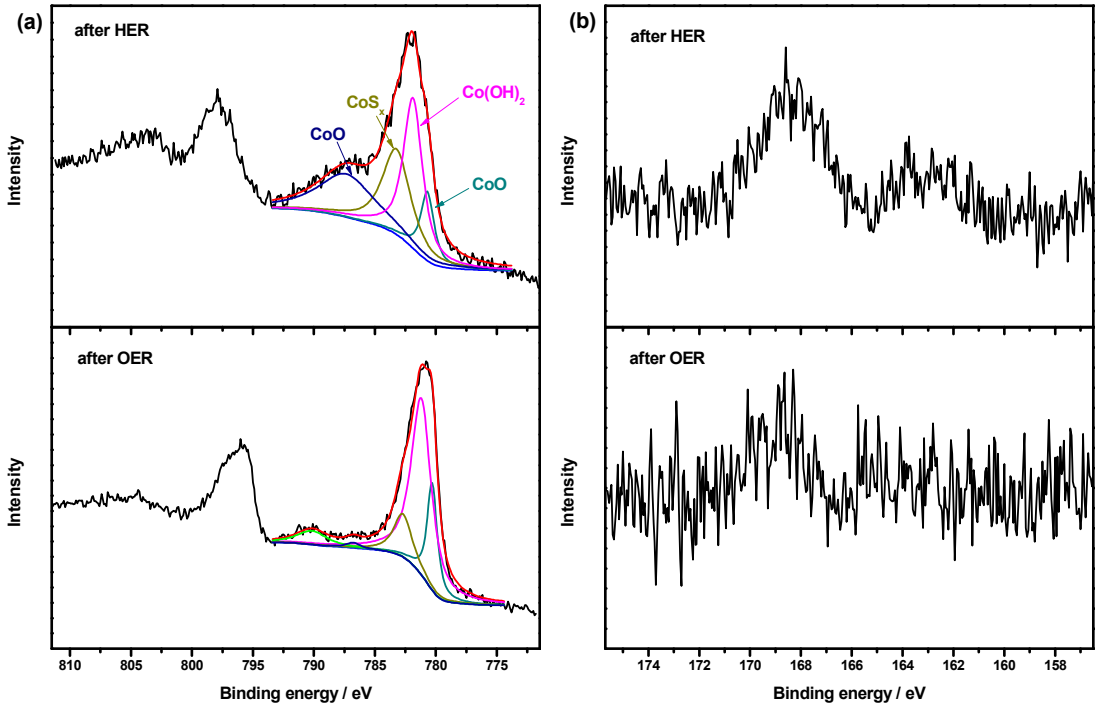

Figure S15. XPS spectra of (a) Co 2p and (b) S 2p for CP/CTs/Co-S after stability test for HER and OER.

In comparison with XPS spectra in Figure S5, the main component in CP/CTs/Co-S after stability test for OER converts to $Co(OH)_2$, consistent with the observations from Figure S14b and S14d.

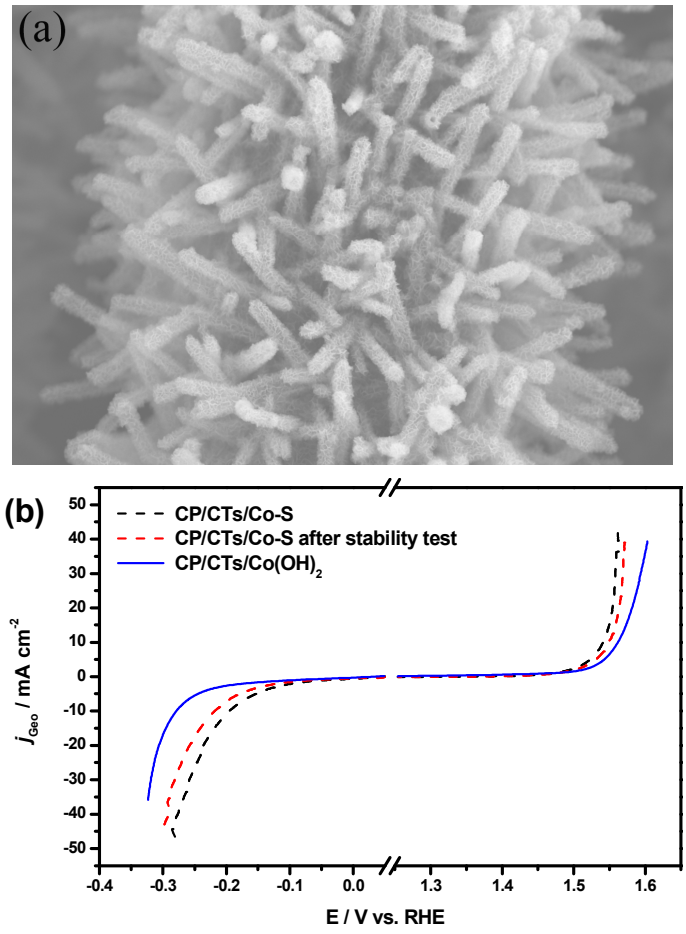

Figure S16. (a) SEM image of CP/CTs/$Co(OH)_2$ and (b) the according HER and OER activities in comparison with CP/CTs/Co-S before and after stability test.

For comparison, CP/CTs/$Co(OH)_2$ was also prepared via the similar electrodeposition method in absence of thiourea with the passed charges equivalent to that of CP/CTs/Co-S. The as-prepared CP/CTs/$Co(OH)_2$ have a similar morphology with CP/CTs/Co-S (Figure S16a). However, as shown in Figure S16b, the HER and OER activities of CP/CTs/$Co(OH)_2$ are even inferior to those of CP/CTs/Co-S after stability test, indicating the advantages of the Co-S composites.

Table S4. Summary of the electrochemical activities of the catalytic electrodes for overall water splitting.

Catalytic electrode		Electrolyte	Loading (mg cm^{-2})	E at j = 10 mA cm^{-2} (V)	Specific activity (mA cm^{-2})	Mass activity (mA mg^{-1})	Reference
Cathode	Anode						
CP/CTs/Co-S		1 M KOH	0.32	1.743	5.1 (1.7 V)	15.9 (1.7 V)	This work
Ni foam/NiFe LDH		1 M NaOH		1.7	20 (~1.78)		Ref. 11
Ni foam/NiO/Ni-CNT	**Ni foam/NiFe LDH**	1 M KOH	8	~1.41	20 (1.5 V) 100 (1.58 V)	2.5 (1.5 V) 12.5 (1.58 V)	Ref. 8
Ni foam/CoO_x@CN	**Ni foam/CoO_x@CN after HER**	1 M KOH	2	~1.32	20 (1.55 V) ~27 (1.7 V)	10 (1.55 V) ~13.5 (1.7 V)	Ref. 9
Ti foil/$Ni_{0.33}Co_{0.67}S_2$ NWs	**Ti foil/$NiCo_2O_4$ NWs**	1 M KOH	0.3	~1.73	~8 (1.7 V)	~26.7 (1.7 V)	Ref. 5
MnNi	**MnNi after thermal modification**	0.1 M KOH	0.28	ΔE= 2.01			Ref. 13
$Ni_{2/3}Fe_{1/3}$-rGO		1 M KOH	0.25	ΔE= ~2.02			Ref. 7
Ni@NC		0.1 M KOH	0.4	ΔE= 1.81			Ref. 12

*The value of ΔE was roughly estimated by adding the absolute potentials of the catalytic electrode at the current density of 10 mA cm^{-2} for HER and OER, respectively.

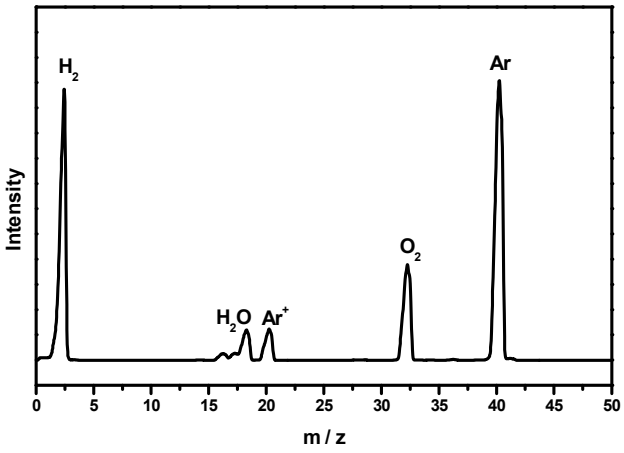

Figure S17. Mass spectrum of the gaseous products from overall water splitting with Ar as carrier gas.

Reference

(1) Sun, Y.; Liu, C.; Grauer, D. C.; Yano, J.; Long, J. R.; Yang, P.; Chang, C. J. Electrodeposited Cobalt-Sulfide Catalyst for Electrochemical and Photoelectrochemical Hydrogen Generation from Water. *J. Am. Chem. Soc.* **2013**, *135*, 17699-17702.

(2) Xiao, P.; Sk, M. A.; Thia, L.; Ge, X.; Lim, R. J.; Wang, J. Y.; Lim, K. H.; Wang, X. Molybdenum Phosphide as an Efficient Electrocatalyst for the Hydrogen Evolution Reaction. *Energy Environ. Sci.* **2014**, *7*, 2624-2629.

(3) Vrubel, H.; Hu, X. Molybdenum Boride and Carbide Catalyze Hydrogen Evolution in both Acidic and Basic Solutions. *Angew. Chem., Int. Ed.* **2012**, *51*, 12703-12706.

(4) Wu, H. B.; Xia, B. Y.; Yu, L.; Yu, X. Y.; Lou, X. W. Porous Molybdenum Carbide Nano-Octahedrons Synthesized *via* Confined Carburization in Metal-Organic Frameworks for Efficient Hydrogen Production. *Nat. Commun.* **2015**, *6*, 6512.

(5) Peng, Z.; Jia, D.; Al-Enizi, A. M.; Elzatahry, A. A.; Zheng, G. From Water Oxidation to Reduction: Homologous Ni-Co Based Nanowires as Complementary Water Splitting Electrocatalysts. *Adv. Energy Mater.* **2015**, *5*, 1402031.

(6) Tian, J.; Liu, Q.; Asiri, A. M.; Sun, X. Self-Supported Nanoporous Cobalt Phosphide Nanowire Arrays: An Efficient 3D Hydrogen-Evolving Cathode over the Wide Range of pH 0-14. *J. Am. Chem. Soc.* **2014**, *136*, 7587-7590.

(7) Ma, W.; Ma, R.; Wang, C.; Liang, J.; Liu, X.; Zhou, K.; Sasaki, T. A Superlattice of Alternately Stacked Ni-Fe Hydroxide Nanosheets and Graphene for Efficient Splitting of Water. *ACS Nano* **2015**, *9*, 1977-1984.

(8) Gong, M.; Zhou, W.; Tsai, M. C.; Zhou, J.; Guan, M.; Lin, M. C.; Zhang, B.; Hu, Y.; Wang, D. Y.;

Yang, J.; Pennycook, S. J.; Hwang, B. J.; Dai, H. Nanoscale Nickel Oxide/Nickel Heterostructures for Active Hydrogen Evolution Electrocatalysis. *Nat. Commun.* **2014**, *5*, 4695.

(9) Jin, H.; Wang, J.; Su, D.; Wei, Z.; Pang, Z.; Wang, Y. In Situ Cobalt-Cobalt Oxide/N-Doped Carbon Hybrids as Superior Bifunctional Electrocatalysts for Hydrogen and Oxygen Evolution. *J. Am. Chem. Soc.* **2015**, *137*, 2688-2694.

(10) Zou, X.; Huang, X.; Goswami, A.; Silva, R.; Sathe, B. R.; Mikmekova, E.; Asefa, T. Cobalt-Embedded Nitrogen-Rich Carbon Nanotubes Efficiently Catalyze Hydrogen Evolution Reaction at All pH Values. *Angew. Chem., Int. Ed.* **2014**, *53*, 4372-4376.

(11) Luo, J.; Im, J. H.; Mayer, M. T.; Schreier, M.; Nazeeruddin, M. K.; Park, N. G.; Tilley, S. D.; Fan, H. J.; Grätzel, M. Water Photolysis at 12.3% Efficiency *via* Perovskite Photovoltaics and Earth-Abundant Catalysts. *Science* **2014**, *345*, 1593-1596.

(12) Ren, J.; Antonietti, M.; Fellinger, T. P. Efficient Water Splitting Using a Simple Ni/N/C Paper Electrocatalyst. *Adv. Energy Mater.* **2015**, *5*, 1401660.

(13) Ledendecker, M.; Clavel, G.; Antonietti, M.; Shalom, M. Highly Porous Materials as Tunable Electrocatalysts for the Hydrogen and Oxygen Evolution Reaction. *Adv. Funct. Mater.* **2015**, *25*, 393-399.

(14) Song, F.; Hu, X. Exfoliation of Layered Double Hydroxides for Enhanced Oxygen Evolution Catalysis. *Nat. Commun.* **2014**, *5*, 4477.

(15) Song, F.; Hu, X. Ultrathin Cobalt-Manganese Layered Double Hydroxide Is an Efficient Oxygen Evolution Catalyst. *J. Am. Chem. Soc.* **2014**, *136*, 16481-16484.

(16) Pintado, S.; Goberna-Ferron, S.; Escudero-Adan, E. C.; Galan-Mascaros, J. R. Fast and Persistent Electrocatalytic Water Oxidation by Co-Fe Prussian Blue Coordination Polymers. *J. Am. Chem. Soc.*

2013, *135*, 13270-13273.

(17)Zou, X.; Goswami, A.; Asefa, T. Efficient Noble Metal-Free (Electro)Catalysis of Water and Alcohol Oxidations by Zinc-Cobalt Layered Double Hydroxide. *J. Am. Chem. Soc.* **2013**, *135*, 17242-17245.

(18)Gao, M.; Sheng, W.; Zhuang, Z.; Fang, Q.; Gu, S.; Jiang, J.; Yan, Y. Efficient Water Oxidation Using Nanostructured α-Nickel-Hydroxide as an Electrocatalyst. *J. Am. Chem. Soc.* **2014**, *136*, 7077-7084.

(19)Li, Y.; Hasin, P.; Wu, Y. $Ni_xCo_{3-x}O_4$ Nanowire Arrays for Electrocatalytic Oxygen Evolution. *Adv. Mater.* **2010**, *22*, 1926-1929.

(20)Koza, J. A.; He, Z.; Miller, A. S.; Switzer, J. A. Electrodeposition of Crystalline Co_3O_4—A Catalyst for the Oxygen Evolution Reaction. *Chem. Mater.* **2012**, *24*, 3567-3573.

(21)Liang, Y.; Li, Y.; Wang, H.; Zhou, J.; Wang, J.; Regier, T.; Dai, H. Co_3O_4 Nanocrystals on Graphene as a Synergistic Catalyst for Oxygen Reduction Reaction. *Nat. Mater.* **2011**, *10*, 780-786.

(22)Gao, M. R.; Xu, Y. F.; Jiang, J.; Zheng, Y. R.; Yu, S. H. Water Oxidation Electrocatalyzed by an Efficient $Mn_3O_4/CoSe_2$ Nanocomposite. *J. Am. Chem. Soc.* **2012**, *134*, 2930-2933.

(23)Ma, T. Y.; Dai, S.; Jaroniec, M.; Qiao, S. Z. Metal-Organic Framework Derived Hybrid Co_3O_4-Carbon Porous Nanowire Arrays as Reversible Oxygen Evolution Electrodes. *J. Am. Chem. Soc.* **2014**, *136*, 13925-13931.

(24)Liu, X.; Chang, Z.; Luo, L.; Xu, T.; Lei, X.; Liu, J.; Sun, X. Hierarchical $Zn_xCo_{3-x}O_4$ Nanoarrays with High Activity for Electrocatalytic Oxygen Evolution. *Chem. Mater.* **2014**, *26*, 1889-1895.